Monthly Notices
of the
ROYAL ASTRONOMICAL SOCIETY

Mon. Not. R. Astron. Soc. **402,** 2609–2616 (2010) doi:10.1111/j.1365-2966.2009.16085.x

Radio emissions from substellar companions of evolved cool stars

Richard Ignace,⋆ Mark L. Giroux and Donald G. Luttermoser

Department of Physics & Astronomy, East Tennessee State University, Box 70652, Johnson City, TN 37614, USA

Accepted 2009 November 18. Received 2009 November 9; in original form 2009 May 8

ABSTRACT

A number of substellar companions to evolved cool stars have now been reported. Cool giants are distinct from their progenitor main-sequence low-mass stars in a number of ways. First, the mass loss rates of cool giant stars are orders of magnitude greater than for the late-type main-sequence stars. Secondly, on the cool side of the Linsky–Haisch 'dividing line', K and M giant stars are not X-ray sources, although they do show evidence for chromospheres. As a result, cool star winds are largely neutral for those spectral types, suggesting that planetary or brown dwarf magnetospheres will not be effective in standing off the stellar wind. In this case, one expects the formation of a bow shock morphology at the companion, deep inside its magnetosphere. We explore radio emissions from substellar companions to giant stars using (a) the radiometric Bode's law and (b) a model for a bow shock morphology. Stars that are X-ray emitters likely have fully ionized winds, and the radio emission can be at the milli-Jansky level in favourable conditions. Non-coronal giant stars produce only micro-Jansky level emissions when adjusted for low-level ionizations. If the largely neutral flow penetrates the magnetosphere, a bow shock results that can be strong enough to ionize hydrogen. The incoherent cyclotron emission is sub-micro-Jansky. However, the long wavelength radio emission of Solar system objects is dominated by the cyclotron maser instability (CMI) mechanism. Our study leads to the following two observational prospects. First, for coronal giant stars that have ionized winds, application of the radiometic Bode's law indicates that long wavelength emission from substellar companions to giant stars may be detectable or nearly detectable with existing facilities. Secondly, for the non-coronal giant stars that have neutral winds, the resultant bow shock may act as a 'feeder' of electrons that is well embedded in the companion's magnetosphere. Incoherent cyclotron emissions are far too faint to be detectable, even with next generation facilities; however, much brighter flux densities may be achievable when CMI is considered.

Key words: stars: late-type – stars: mass-loss – planetary systems – radio continuum: stars.

1 INTRODUCTION

The discovery of extrasolar planets around solar-type stars has now become a fairly regular occurrence (e.g. see the Extrasolar Planets Encyclopaedia maintained by J. Schneider at www.obspm.fr/encycl/encycl.html). In addition to these, there have now been numerous detections of planetary companions to cool *giant* stars, (early detections include Frink et al. 2002; Setiawan et al. 2003, and Sato et al. 2003). With the ansatz that the formation of planetary systems around solar type stars is a relatively common occurrence, plus the recognition that such stars will evolve to become giants that experience significant mass loss on the way to becoming white dwarf stars, it becomes interesting to consider how giant star winds might affect substellar companions.

⋆E-mail: ignace@etsu.edu

This paper is not the first to entertain questions about the eventual evolution of planetary systems during late stellar phases. Several authors have considered the angular momentum transfer between the orbit of a planet or brown dwarf with a red giant and/or its wind (Livio & Soker 1984; Soker, Livio & Harpaz 1984; Livio & Soker 2002). Such effects could lead to 'sculpting' of planetary nebulae (e.g. Soker 2001), which could explain the non-spherical but axisymmetric shapes that are so commonly observed (e.g. Balick 1987). Rasio et al. (1996) have discussed the tidal decay of planetary orbits during the red giant phase. Indeed, even as far back as 1924, Jeans examined the evolution of binary orbits due to stellar mass-loss (only in that paper, the mass-loss being considered was in the form of the conversion of matter to energy via nuclear fusion). Moreover, several authors have considered the possibility of detecting planetary companions to white dwarf stars, with the goal of constraining the evolution of planetary systems through empirical means (Zuckerman & Becklin 1987; Livio, Pringle & Saffer 1992;

Li, Ferrario & Wickramasinghe 1998; Chu et al. 2001; Ignace 2001; Burleigh, Clarke & Hodgkin 2002). Recently, a substellar companion to a subdwarf in a post-red giant phase of evolution was reported (Geier et al. 2009). This is particularly interesting as an example of a low-mass companion that avoided being engulfed by the bloated red giant star to survive in a small period orbit around the remnant. Such occurrences bolster the need for the consideration of detecting substellar companions to red giants to understand better the connections between stellar evolution and planetary evolution.

In this contribution, one single fact is emphasized: when stars like the Sun evolve to become red giants, the mass-loss increases substantially by several orders of magnitude which may have observational consequences for detecting substellar companions and detailing their physical and orbital properties. Already the influence of a strong wind on a substellar companion has been considered by Struck, Cohanim & Willson (2004), who discuss the possibility of wind accretion by brown dwarf companions during the asymptotic giant branch (AGB) phase.

In terms of detecting extrasolar planets, a number of researchers have explored radio emissions from substellar companions to stars by extrapolating the radio properties of Solar system planets to other star systems (e.g. see Zarka 2007 and references therein). The radio emission of the Earth and other Solar system planets with significant magnetic fields are dominated by the cyclotron maser instability (CMI) process in which the low frequency spectrum below about 100 MHz is dominated by coherent cyclotron emission from mildly relativistic electrons (Gurnett 1974). A key point is that electrons are fed to the magnetic poles where the CMI is strong, and that the coherent cyclotron emission dominates the incoherent emission by several orders of magnitude. A greater understanding of the detailed energetics and emissive mechanism has come about fairly recently in relation to the terrestrial auroral kilometric radiation (AKR) by Mutel et al. (2007) and Mutel, Christopher & Pickett (2008).

In applications to extrasolar planets, Jupiter has been prominent in these considerations, since it shows bursting behaviour in the radio band that can be quite bright, partly in relation to interactions occurring between Jupiter and Io (e.g. Zarka 1998, 2004). Griessmeier, Zarka & Spreeuw (2007) have summarized various mechanisms that may contribute to radio emissions in the case of exoplants around main-sequence stars. For example, coronal mass ejections and in some cases magnetic field interactions between the star and a short-period planet can produce strong radio signals. Our contribution is to extend the use of the radiometric 'Bode's Law' for late-type main-sequence stellar winds to those of giant stars for which several new considerations must be taken into account. This law is an empirically determined, and theoretically motivated, power-law relation between planetary radio emissions and the solar wind kinetic energy flux. The radio emissions occur at low frequencies of about 0.3–40 MHz, of which the upper end is observable with the Low Frequency Array (LOFAR) (Farrell et al. 2004). A lunar radio observatory such as the proposed Dark Ages Lunar Interferometer (DALI) would be sensitive to almost that entire range (see Lazio et al. 2007 for a summary of the capabilities of lunar based radio observatories).

Giant star winds differ from those of low-mass main-sequence stars (i.e. solar-type winds) in important ways. Giants that are warmer than early K tend to be X-ray emitters, whereas those that are cooler are X-ray faint. The distinction in the X-ray properties is known as the Linsky–Haisch 'dividing line' (Linsky & Haisch 1979). Although these X-ray faint giants possess chromospheres, their winds are largely neutral (e.g. Reid & Menten 1996), whereas the earlier giants and the winds of low-mass main-sequence stars are ionized plasma flows. Consequently, in the case of the neutral giant star winds, the flow can *penetrate* the magnetosphere of a substellar companion, and the supersonic wind flow will set up a bow shock in the vicinity of that companion. Cassinelli et al. (2008) have considered a closely related scenario. Interested in X-ray emissions, those authors used hydrodynamic simulations to model the bow shock for an early-type stellar wind interacting with a dense spherical gaseous clump. With a wind speed of order 10^3 km s^{-1}, and assuming adiabatic cooling, they were able to derive a power-law dependence for the differential emission measure with temperature of the form $\mathrm{d}EM/\mathrm{d}T \propto T^{-7/3}$, with peak hot gas temperatures of order 10^7 K.

That simulation remains relevant for the case of a substellar companion to a cool giant star. Although cool star winds are far slower than hot star winds, with values of 15 km s^{-1} for AGB stars up to perhaps 100 km s^{-1} for some red giants, the winds are themselves much cooler, with sound speeds of a few km s^{-1}. As a result, the wind is still quite supersonic.

However, this does not mean that bow shocks to substellar companions will produce X-ray emissions for the cooler giant star systems. These winds are indeed much slower than those of early-type stars, and so the peak post-shock temperature will be considerably smaller. For a strong shock, as considered by Cassinelli et al., the post-shock temperature at the bow shock head (or 'apex') T_A follows the well-known Rankine–Hugoniot relation, with

$$T_A = \frac{3}{16}\,\frac{\mu m_{\rm H}}{k}\,v_{\rm rel}^2 = 14\,{\rm MK}\,\left(\frac{v_{\rm rel}}{1000\ {\rm km\ s^{-1}}}\right)^2. \qquad (1)$$

where μ is the mean molecular weight for the gas, $m_{\rm H}$ is the mass of hydrogen, and $v_{\rm rel}$ is the relative speed between the wind and the companion. The orbital motion can be non-trivial compared to the wind, but considering only the wind speed for the moment, one expects apex temperatures on the order of $T_A \approx$ 3000–140 000 K for speeds of 15–100 km s^{-1}. At the low end, orbital motion will likely dominate the incident shock speed in the rest frame of the companion (e.g. the Earth orbits at about 30 km s^{-1}). As a result, post-shock temperatures of $\sim 10^4$–10^5 K are expected, sufficient to ionize hydrogen, thus leading to a substantial reservoir of electrons that can interact with a magnetosphere to produce radio emissions.

The scenario for the giant stars is thus significantly different than for main sequence stars. First, known low-mass companions to giants have no examples of extremely short period orbits (a week or less) as in the main sequence case. Secondly, giants with the most massive winds will be neutral, and thus have no counterpart in the Solar system or to current applications among late-type main sequence stars. Thirdly, for the X-ray emitters (or 'coronal' giants), there has been no evidence for coronal mass ejections as in the solar case, so that the application of the radiometric Bode's law is likely the most important emissive mechanism in the long wavelength radio band. It is worth noting that Griessmeier et al. (2007) have evaluated the expected radio emissions for all known exoplanets at that time. Their list includes companions to giant stars that had been reported at that time, and these do not produce detectable radio emissions. However, those authors appear to have applied a main-sequence solar wind model in relation mass-loss rate and wind speed which is inapplicable to giant star winds. Here, we use empirical relations that are more appropriate for evolved cool star winds.

To explore the radio emissions from companions to giant stars, the next section summarizes the properties of the host stars and the orbital properties of their companions. In Section 3, we apply the radiometric Bode's law to giant star systems, comparing emissions between stars on either side of the Linsky–Haisch dividing line.

In Section 4, we consider the bow shock scenario for the case of neutral winds that penetrate deep into a magnetosphere. We use the results of Cassinelli et al. (2008) to estimate the incoherent cyclotron emission. Results of our study are summarized in Section 5, where we conclude that new simulations are required to consider properly the operation of the CMI in the bow shock scenario. Appendix A details our derivation for the cyclotron emission from a bow shock.

2 GIANT STARS AND THEIR SUBSTELLAR COMPANIONS

A large number of substellar companions have been identified in radial velocity surveys of giant stars. From the literature, we have gathered information about their physical properties which are displayed in Table 1. Distances were taken from the SIMBAD data base that lists values from the *Hipparcos* survey. References for the stellar and planetary properties appear in the last column. Note that some of the values in the table are quite uncertain, and the reader is strongly urged to consult the references for further details of their evaluation. Our goal here is to use these values as a guide for our application to the radio emissions.

With these stellar parameters we use a standard form of Reimer's law to estimate wind mass-loss rates $\dot{M}$ (Reimers 1975; Lamers & Cassinelli 1999),

$$\dot{M} = 4 \times 10^{-13}\, \eta\, \frac{(L_*/\mathrm{L}_\odot)\,(R_*/R_\odot)}{(M_*/\mathrm{M}_\odot)}\, \mathrm{M}_\odot\ \mathrm{yr}^{-1}, \qquad (2)$$

where η is a scaling parameter between about 0.3 and 3. Here, we adopt $\eta = 1$ since only mass-loss rate estimates will be needed. Computed mass-loss rate values are given in Table 1 in the seventh column, scaled to $10^{-9}\,\mathrm{M}_\odot\ \mathrm{yr}^{-1}$. Note that no value is given for HD13189 since no radius or temperature value was quoted for this star.

The mass-loss is important since it sets the scale of the wind density at the companion where radio emission will be produced. Table 1 shows that there is a significant spread in values fro the giants with planets detected so far, ranging from $4 \times 10^{-8}\,\mathrm{M}_\odot\ \mathrm{yr}^{-1}$

Table 1. Nominal stellar and planetary data on evolved stars with planetary companions.

	Host star data						Planet data			
Name	Spectral type	Distance (pc)	Mass ($\mathrm{M}_\odot$)	Radius ($\mathrm{R}_\odot$)	Luminosity ($\mathrm{L}_\odot$)	$\dot{M}$ ($10^{-9}\,\mathrm{M}_\odot\ \mathrm{yr}^{-1}$)	$M \sin i$ (M_J)	a (au)	e	Ref.[a]
HD185269	G0 IV	47	1.28	1.88	4.0[b]	0.002	0.94	0.077	0.30	J06
81 Cet	G5 III:	97	2.4	11	60	0.11	5.3	2.5	0.206	S08b
HD 11977	G5 III	67	1.91	10	55[b]	0.12	6.54	1.93	0.4	Se05
18 Del	G6 III	73	2.3	8.5	40	0.059	10.3	2.6	0.08	S08a
11 Com	G8 III	112	2.7	19	170	0.48	19.4	1.29	0.231	L08
HD175541	G8 IV	128	1.65	3.80	8.6	0.008	0.61	1.03	0.33	J07
HD192699	G8 IV	67	1.68	3.9	10.2	0.009	2.5	1.16	0.149	J07
HD 104985	G9 III	102	1.6	11	59	0.16	63	0.78	0.03	Sa03
ξ Aql	K0 III	63	2.2	12	69	0.15	2.8	0.68	0[d]	S08a
ϵ Tau	K0 III	47.5	2.7	14	97	0.20	7.6	1.93	0.151	S07
HD102272	K0 III	360	1.9	10.1	53[b]	0.11	5.9	0.61	0.05	N09b
14 And	K0 III	76	2.2	11	58	0.12	4.8	0.83	0[d]	S08b
HD17092	K0 III	110	2.3	10.1	43[b]	0.076	4.6	1.3	0.17	N07
β Gem	K0 III	10.3	1.86	9	34[b]	0.066	2.9	1.69	0.06	H06, R06
HD81688	K0 III-IV	88	2.1	13	72	0.18	2.7	0.81	0[d]	S08a
κ Cr B	K0 IV	31.1	1.8	4.71	12.3	0.013	1.8	2.7	0.146	J08
6 Lyn	K0 IV	57	1.7	5.2	15	0.018	2.4	2.2	0.134	S08b
HD32518	K1 III	120	1.13	10.2	41[b]	0.15	3.04	0.59	0.01	D09b
4 U Ma	K1 III	62	1.23	18	110[b]	0.64	7.1	0.87	0.43	D07
HD167042	K1 III	50.	1.64	4.30	10.5	0.011	1.7	1.3	0	J08
HD 47536	K1 III	121	1-1.5	23	4380	40	5-6	2	0.20	Se03
HD167042	K1 IV	50	1.5	4.5	10	0.012	1.6	1.3	0.101	S08b
γ Ceph	K1 IV	13.8	1.6	4.66	11[b]	0.013	1.7	2.13	0.12	H03
HD210202	K1 IV	56	1.85	4.45	11.3	0.011	2.0	1.17	0.152	J07
42 Dra	K1.5 III	97	0.98	22	130[b]	1.2	3.88	1.19	0.38	D09a
BD +20 2457	K2 II	200+[c]	2.8	49	610[b]	4.3	21.42	1.45	0.15	N09a
BD +20 2457	K2 II	200+[c]	2.8	49	610[b]	4.3	12.47	2.01	0.18	N09a
HD 13189	K2 II?	—	2-7	—	4000	—	8-20	1.5-2.2	0.27	H05
ι Dra	K2 III	31	1.05	12.9	70	0.34	8.9	1.3	0.70	F02
HD24210	K3 III	140	1.25	56	950[b]	17	6.90	1.33	0.15	N09
HD139357	K4 III	118	1.35	11.5	58[b]	0.20	9.76	2.36	0.10	D09a
11 U Mi	K4 III	120	1.8	24	180[b]	0.96	11.2	1.54	0.08	D09b

[a]References: D09 = Dollinger et al. (2009b); D09a = Dollinger et al. (2009a); N09a = Niedzielski et al. (2009a); L08 = Liu et al. (2008); S08a = Sato et al. (2008a); S08b = Sato et al. (2008b); S07 = Sato et al. (2007) N09b = Niedzielski et al. (2009b); N07 = Niedzielski et al. (2007); D07 = Dollinger et al. (2007); J06 = Johnson et al. (2006); Se05 = Setiawan et al. (2005); H05 = Hatzes et al. (2005); Sa03 = Sato et al. (2003); F02 = Frink et al. (2002); Se03 = Setiawan et al. (2003); H06 = Hatzes et al. (2006); R06 = Reffert et al. (2006); H03 = Hatzes et al. (2003); J07 = Johnson et al. (2007); J08 = Johnson et al. (2008).

[b]Luminosity computed from values of T_eff and $\log g$ given by respective reference.

[c]Luminosity estimate based on spectral type.

[d]Eccentricity fixed to zero for orbital solution.

for HD47536 down to about $10^{-12}\,M_\odot\ yr^{-1}$ for the subgiant HD185269. However, there is controversy about the Reimer's law and its applicability. An understanding of it remains a topic of current research (e.g. Schröder & Cuntz 2005). The law has application to more luminous cool stars, but its extension to their lower luminosity cousins is less clear. Also ongoing are attempts to understand the Linsky–Haisch 'dividing line' that separates giant stars earlier than about K0 that show X-ray emissions from the later types that are not coronal but which do have chromospheres (Suzuki 2007). Again, the main value of Table 1 is the determination of representative stellar and planetary parameters and their spread for the sample as a whole.

In relation to the population of host giant stars, the notable points are that the median distance is around 100 pc, about 10 times farther than main sequence host stars of substellar companions. Also, the mass-loss rates are typically of order $10^{-10}\,M_\odot\ yr^{-1}$, about 4 orders of magnitude larger than the solar wind, but lower by a similar factor from the AGB winds. Finally, the distribution of orbital semi-major axes and eccentricities reflects the selection effects of the radial velocity study: values of a around 1 au or less, and values of e that can deviate significantly from circular orbits.

3 APPLICATION OF THE RADIOMETRIC BODE'S LAW TO GIANT STAR WINDS

Radio studies of single red giant stars reveal them to be faint radio emitters (Spergel, Giuliani & Knapp 1983; Reid & Menten 1996; Güdel 2002). For the brighter sources, observations at different radio bands indicate a flux density spectrum of the form $S_\nu \propto \nu^2$, consistent with the Rayleigh–Jeans limit and suggestive of photospheric emission, although there are some exceptions indicating extended radio photospheres.

The main conclusion is that the red giant star winds that show chromospheric signatures but not coronal X-rays are largely neutral, yet some metals are ionized, resulting in low level ionizations of the wind material at the level of 0.01–0.1 per cent (Reid & Menten 1996). These ionizations are 3–4 orders of magnitude below that of the Sun's wind. However, the mass-loss rate from giant stars is four or more orders of magnitude larger than the solar wind. Interestingly, Judge & Stencel (1991) have reported on larger ionizations in some red giant stars. It is true that the earlier red giants, earlier than about K2 that show X-ray emissions, have fully ionized winds. Unfortunately, their mass-loss rates are relatively uncertain. It is useful to consider how even the paltry ionized component of a giant star wind might interact with planetary magnetospheres so that at least lower limits to the radio emissions may be derived.

The topic of radio emissions in the Solar system and from extrasolar planets has been studied extensively. To estimate the flux density from the giant star wind impinging on a planetary magnetosphere, we use the radiometric 'Bode's' law of equation (3) from Lazio et al. (2004) based on scaling relations from Farrell, Desch & Zarka (1999) and Zarka et al. (2001). The median radio power from the stellar wind interaction with the planet is

$$L \approx 4\times10^{18}\ \mathrm{erg\ s^{-1}} \left(\frac{\omega}{\omega_\mathrm{J}}\right)^{0.79} \left(\frac{M}{M_\mathrm{J}}\right)^{1.33} \left(\frac{d}{5\,\mathrm{au}}\right)^{-1.6} \times \left(\frac{\rho\, v_\mathrm{w}^3}{\rho_\odot\, v_\odot^3}\right), \quad (3)$$

where ω is the planet's rotation rate, M is its mass, d is the orbital distance of the planet from its star, ρ and v_w are the density and speed of the stellar wind, $\rho_\odot$ and $v_\odot$ are the density and speed of the solar wind, and 'J' subscripts indicate values for Jupiter. The density ρ must be corrected for the lower ionization level of a late giant star wind as compared to a main-sequence star. Introducing η as a ratio of stellar wind properties to that of the Sun, and assuming a spherically symmetric wind with $\rho = q\dot{M}/4\pi d^2 v_\mathrm{w}$, we can derive that

$$\eta = \frac{q\dot{M}\, v_\mathrm{w}^2}{\dot{M}_\odot\, v_\odot^2}, \quad (4)$$

where q is the ionization correction factor, with a value of about 10^{-4} to 10^{-3}. With $\dot{M}_\odot \approx 10^{-14}\,M_\odot\ yr^{-1}$ and $v_\odot \approx 400\ km\ s^{-1}$ for the Sun, and $\dot{M} \approx 10^{-8}\,M_\odot\ yr^{-1}$ and $v_\mathrm{w} \approx 30\ km\ s^{-1}$ for a giant star wind with $q = 10^{-3}$, we arrive at $\eta \sim 6$ for a red giant with fairly strong mass loss. Some red giants have lower $\dot{M}$ values and faster speeds, in which case η would remain comparable to the above value. AGB stars on the other hand are slower by a factor of 2 but have higher mass loss by a factor of 10^3, and so η can become quite large at around 10^3.

Assuming $\eta \sim 10$, and the other scaling ratios are unity in equation (3), then the total radio luminosity would be approximately $4\times10^{19}\ erg\ s^{-1}$. Using equation (4) of Lazio et al. for a typical emission frequency of $\nu \sim 25$ MHz, combined with their equation (5) for the flux density under the approximation that the radio luminosity is emitted isotropically in a bandwidth of $\Delta\nu \approx \nu/2$, the expected radio brightness level will be

$$\begin{aligned} S_\nu &\approx \frac{L}{4\pi\,(\nu/2)\,D^2} \\ &\approx 1.0\,\mu\mathrm{Jy}\,\frac{q}{10^{-3}} \left(\frac{\omega}{\omega_\mathrm{J}}\right)^{-0.21} \left(\frac{M}{M_\mathrm{J}}\right)^{-0.33} \left(\frac{d}{1\,\mathrm{au}}\right)^{-1.6} \\ &\quad\times \left(\frac{\nu}{12.5\,\mathrm{MHz}}\right)^{-1} \left(\frac{\Omega}{4\pi}\right)^{-2} \left(\frac{D}{100\,\mathrm{pc}}\right)^{-2} \left(\frac{\dot{M}}{10^{-8}}\right) \\ &\quad\times \left(\frac{v_\mathrm{w}}{30}\right)^{2} \left(\frac{R}{R_\mathrm{J}}\right)^{-3}, \end{aligned} \quad (5)$$

where D is the Earth–star distance, and Ω is the beaming of the radiation relative to isotropic. If all of the parenthetical factors were unity, then a Jupiter-like companion to a red giant star at 100 pc would have a flux density of $S_\nu \approx 1$ μJy. This is too faint for detection by current or near-future radio telescopes.

However, it should be noted that we have assumed nearly neutral winds, referring to late red giants, those that lie on the cool side of the Linsky–Haisch dividing line. Red giants of earlier spectral type that are X-ray emitters likely have winds similar to that of the Sun, namely fully ionized plasmas. For such stars $q \approx 1$, with a gain factor in the radio emission of 3 orders of magnitude, bringing the flux density up to about 1 mJy, which is within the realm of detection by facilities such as LOFAR.

Unfortunately, most giant stars that are known host stars for substellar companions have much lower mass-loss rate values than assumed in equation (5), closer to $10^{-10}\,M_\odot\ yr^{-1}$. For an ionized red giant wind with $q = 1$, this level of mass-loss pushes the expected flux density down to about 10 μJy, again well below detection thresholds. However, some G giants can have $\dot{M}$ values closer to $10^{-9}\,M_\odot\ yr^{-1}$ (e.g. 11 Com in Table 1). It is easy to imagine favourable cases with an early giant star wind with somewhat large mass-loss and higher wind speed along with a companion in a sub-au orbit (possibly eccentric – see Section 5) that could return the radio flux density closer to the mJy level.

In addition, it is possible that in fact the majority of giant stars maintain planetary systems or brown dwarf companions. Substantially higher radio flux densities would then be expected from

giants with higher mass-loss rates, ones that have not been included in the radial velocity surveys. For example, AGB stars with $\dot{M} \gtrsim 10^{-7}\,\mathrm{M}_{\odot}\ \mathrm{yr}^{-1}$ could represent a new stellar population for detecting substellar companions in later stages of stellar evolution than has so far been targeted.

4 RADIO EMISSION FROM A WIND BOW SHOCK

We now turn to a new consideration for generating radio emissions. Since some giant star winds are neutral, they will penetrate companion magnetospheres and can be expected to set up bow shocks in close vicinity of the substellar object. Cassinelli et al. (2008) describe a hydrodynamic simulation of a massive star wind impinging on a spherically symmetric 'hard' clump. For these authors, the focus was on explaining X-ray emissions from hot star winds. But the key results of the simulations pertain to emission measure and temperature distributions, and so the results have relevance for bow shocks formed from red giants that intercept substellar companions. To explore the observational consequences of this scenario, we adopt expressions for the emission measure (EM) distribution of post-shocked gas as a function of temperature (T) from equations (23) and (24) of Cassinelli et al. (2008),

$$\frac{\mathrm{d}EM}{\mathrm{d}T} = \frac{EM_0}{T_A}\left(\frac{T}{T_A}\right)^{-7/3}, \tag{6}$$

where T_A is given from equation (1). The emission measure scaling factor EM_0 is set by the square of the wind number density (times four owing to a strong shock) at the location of the companion multiplied by the volume of the companion. Its value is given by

$$EM_0 = 1.4\times10^{46}\,\mathrm{cm}^{-3}\left(\frac{R}{10^{10}}\right)^3\left(\frac{\dot{M}_{-8}}{\mu\, v_{30}\, r_{\mathrm{au}}^2}\right)^2, \tag{7}$$

with R the planet radius, $\dot{M}_{-8}$ the wind mass-loss rate divided by $10^{-8}\,\mathrm{M}_{\odot}\ \mathrm{yr}^{-1}$, v_{30} the radial wind speed divided by 30 km s^{-1}, and r_{au} the orbital distance of the planet in au. Note that the EM is a strong function of the planet size (as the cube) and the orbital distance (as the fourth power). The sizes of Jovian planets and brown dwarfs vary slowly with radius, except for short-period companions where X-ray and ultraviolet heating and tidal effects can enlarge the effective radius of the planet (e.g. Guillot et al. 1996; Lammer et al. 2003; Burrows et al. 2007). We assume a nominal value of $R \approx 10^{10}$ cm.

The scenario that we envision is one where the largely neutral wind penetrates a planetary or brown dwarf magnetosphere. On the scale of the companion size, the wind flow is approximately plane parallel as in the Cassinelli et al. (2008) simulation for a wind clump. The peak temperature achieved at the bow head will be of order 10^4 K or more. The hydrogen gas can become ionized, and the bow shock has a decreasing temperature distribution along its length downstream. The shock becomes increasingly oblique until it drops down to around 3000 K, where we assume that hydrogen is no longer ionized at the shock front.

This reservoir of electrons finds itself embedded deep inside a magnetosphere that is sweeping past them. Ignoring the details of the flow dynamics, we make a lower limit estimate for the radio emission as arising from a non-relativistic, incoherent cyclotron process. This emission will occur at a characteristic frequency of

$$\nu_{\mathrm{c}} = \frac{e\,B}{2\pi m_{\mathrm{e}} c}, \tag{8}$$

which is about 28 MHz for a field strength of 10 G. In fact, the emission occurs within the volume of the bow shock, predominantly in a higher density region that hugs the bow shock itself (see Cassinelli et al. 2008). A derivation for the flux density and spectral shape of the thermal, non-relativistic cyclotron emission is given in the Appendix. The result is reproduced here (see equation A15), with the flux density

$$S_\nu \sim 0.3\ \mu\mathrm{Jy}\left(\frac{B_0}{30\,\mathrm{G}}\right)\left(\frac{T_A}{30\,000\,\mathrm{K}}\right)\left(\frac{EM_0}{1.4\times10^{46}}\right) \times\left(\frac{n_{\mathrm{e}}}{5.7\times10^7}\right)^{-1}\left(\frac{D}{100\,\mathrm{pc}}\right)^{-2}\left(\frac{\nu}{\nu_A}\right)^{1/3} x^{2/3}\,\xi^{-1}, \tag{9}$$

where $x = T/T_A$, and $\xi = \xi(x)$ as described in equations (A12) and (A13) of the Appendix. The scale of this emission is sub-micro-Jansky, well below the detectability of current instrumentation. However, there are several key points to note. First and foremost, the above calculation should be considered as a minimum flux density in the sense that it does not take account of CMI or any bursting behaviour such as is observed in Jupiter, and such emissive processes will be stronger by orders of magnitude over the thermal cyclotron emission that we have considered. Nor does it account for the possible influence of moons, each of which would have its own bow shock. (Of course, being a smaller target, the overall EM from a moon's bow shock would be much smaller than for a Jovian-like object, yet the shock could have hotter gas owing to its circumplanetary orbital motion.) The ionization is set only by the relative flow between the blunt object and the wind. Although the EM of the bow shock for a moon would be insignificant as compared to the companion bow shock, its primary influence may be in the form of providing an injection mechanism of electrons to the polar field regions of the companion where the CMI operates.

It should be noted that much of what is being proposed for the bow shock is qualitative only. For a magnetosphere with a typical field strength of order 10 G in the vicinity of the bow shock, the magnetic energy density $U_B = B^2/8\pi \sim 4$ erg cm^{-3} is vastly larger than the ram pressure of the wind flow $\rho v^2 \approx 10^{-3}$ erg cm^{-3}. The implication is that a very strong field is rotating past the bow shock, that in essence acts as an ionization front. The post-shocked plasma is essentially being 'slammed' by the magnetosphere and rapidly accelerated. It is unclear what effect this will have on the bow shock structure itself. A fully consistent MHD simulation of this scenario needs to be carried out. It is a situation unlike anything occurring in the Solar system where the solar wind is everywhere extremely fast and highly ionized in its interactions with Solar system bodies. Importantly, it is unclear in the neutral giant wind case how or if electrons can be accelerated to mildly relativistic values and also channelled to the polar regions of the field axis for the CMI to operate.

However, it is encouraging that there is current interest in both theoretical and experimental work for understanding the CMI process. For example, McConville et al. (2008) conducted a laboratory experiment for a scaled version of the terrestrial AKR that yielded results in basic agreement with satellite measurements. Their work revealed that approximately 1 per cent of the electron kinetic energy pool was converted to radiation via the CMI. These results appear reproducible in 3D numerical simulations (Gillespie et al. 2008). Such work supports the ansatz that a similar level of efficiency can be used in applications to extrasolar planets (e.g. Jardine & Cameron 2008). To advance modelling of the radio emissions in the red giant wind case, MHD simulations will be necessary to assess how electrons can be fed to the magnetic poles of the companion, and then combine that information with the body of work just described for the AKR mechanism. It seems likely that such an approach will be tractable.

5 DISCUSSION

On the whole our analysis for the detection of radio emissions from the interaction between the wind of a red giant star and its substellar companion is largely negative. Cyclotron emissions appear to be at the micro-Jansky level, orders of magnitude below current or near-future detection thresholds. However, we have taken the most conservative and pessimistic approach in our estimates. We have considered red giant winds that are largely neutral (i.e. those on the cool side of the 'dividing line'), yet the winds of earlier type red giants may be highly ionized with large gain factors in the resultant radio emissions.

There have been radio-wavelength surveys (typically at 2 and 6 cm) of red giant stars including stars on the AGB of the Hertzsprung–Russell diagram (see Drake & Linsky 1983, 1986; Drake, Linsky & Elitzer 1987; Drake et al. 1991; Luttermoser & Brown 1992). Typically evolved stars on the cool side of the 'dividing line' are either not detected at these wavelengths or are very weak sources – giant stars of M6 or warmer have been detected (Drake et al. 1991). The weak radio emission of these non-Mira giants are thought to be due to partially ionized winds. There have been some detections of giants on the cool side of M6 III. For example *o* Ceti (Mira) appears variable in its radio emission. Mira was detected at 6 cm by Spergel et al. (1983) as a 3σ event; however, Drake et al. (1987) failed to detect this pulsating long-period variable at either 2 or 6 cm. Since Mira has a hot companion, it is not clear if the emission arose from the long-period variable or from the companion. In a survey of seven N-type carbon stars at 3.6 cm, Luttermoser & Brown (1992) only detected V Hya, which is a peculiar carbon star that shows evidence of bipolar outflow (Tsuji et al. 1988).

In the case of a neutral wind, we have argued that a bow shock will result in the vicinity of the companion object. If the relative flow speed is enough, one can expect post-shock ionization of the wind material. For incoherent cyclotron emission, the radio flux of the ionized component will be quite weak. However, it may be possible that some fraction of these newly created electrons are fed to the polar regions of the companion where the CMI mechanism can operate leading to much stronger radio emission. In addition, analogous to the Jupiter–Io interaction, moons of substellar companion may also produce bow shocks, and these might provide a source of electrons that could be accelerated in the magnetosphere and feed the CMI. Our model for the bow shock is not adequate to address these possibilities. New self-consistent MHD calculations will be needed to model the interaction of the bow shock with the companion's magnetosphere and to assess the channelling of electrons for use with the CMI.

Of course, all of the effects described so far would be affected by orbital eccentricity of the companion. For orbits of a fixed semi-major axis, the radio flux density will be significantly higher near periapse as compared to apapse for increasingly eccentric orbits. But then of course, gains in signal strength near periapse will occur over a diminishing fraction of the orbital period as eccentricity increases. Although these effects should be explored, they are of secondary importance to substantial task of modelling the flow dynamics more accurately.

Finally, it is possible that the AGB stars might be targeted for long wavelength radio studies. The AGB winds are certainly neutral so that the bow shock scenario would be of interest. The mass-loss rates can be extremely large at around $10^{-5}\,\mathrm{M}_{\odot}\ \mathrm{yr}^{-1}$. Since the radio emission scales with $\dot{M}^2$, there would be a gain factor of 6 orders of magnitude above our estimates for the radio emission, and that is just for incoherent cyclotron emission. Of course, AGB stars are relatively rare and so tend to be more distant. Plus the companion will probably need to be in an orbit that is greater than 1 au, otherwise it could be engulfed by the star. With a wind speed of just 15 km s^{-1}, the astute reader may recognize that the apex temperature will hardly be large enough to ionize hydrogen. However, there are actually two effects to mitigate the low wind speed. First is that the orbital speed could be larger by perhaps a factor of 2 or more. Secondly, the hydrodynamical simulations of Cassinelli et al. (2008) are for clumps treated as blunt obstacles without self-gravity. Jovian and brown dwarf mass objects have surface escape speeds of 30 km s^{-1} and higher. Given that the bow shock apex is at around 1.5 times the radius of the blunt object in the Cassinelli et al. simulations, a slow AGB wind can double and triple in speed as it falls into the gravitational potential of the substellar companion (i.e. similar to accretion described by Bondi & Hoyle 1944). Of course, inclusion of gravity changes the details of the bow shock, but the main point is that significant ionization would still be viable. Collecting the various factors, S_ν of around 0.1 mJy might be achievable.

It is clear that long wavelength observations will provide new opportunities for detecting substellar companions and for studying their magnetospheres. Companions to red giants should not be neglected in these efforts. An interesting result of our study has been the relatively novel consideration of neutral winds interactions with substellar companions, completely unlike the Solar system case. The prospects for future observations are certainly exciting, but there is a clear need for more detailed modelling of MHD bow shocks in relation to the CMI to explore the viability of radio detection.

ACKNOWLEDGMENTS

The authors are gratefully indebted to Bob Mutel for discussions that clarified the AKR process as well as an anonymous referee whose comments led to improvements of this paper. This research has made use of the SIMBAD data base, operated at CDS, Strasbourg, France.

REFERENCES

Balick B., 1987, AJ, 94, 671
Bondi H., Hoyle F., 1944, MNRAS, 104, 273
Burleigh M. R., Clarke F. J., Hodgkin S. T., 2002, MNRAS, 331, L41
Burrows A., Hubeny I., Budaj J., Hubbard W. B., 2007, ApJ, 661, 502
Cassinelli J. P., Ignace R., Waldron W. L., Cho J., Murphy N. A., Lazarian A., 2008, ApJ, 683, 1052
Chu Y.-H., Dunne B. C., Gruendl R. A., Brandner W., 2001, ApJ, 546, L61
Dollinger M. P., Hatzes A. P., Pasquini L., Guenther E. W., Hartmann M., Girardi L., Esposito M., 2007, A&A, 472, 649
Dollinger M. P., Hatzes A. P., Pasquini L., Guenther E. W., Hartmann M., Girardi L., 2009a, A&A, 499, 935
Dollinger M. P., Hatzes A. P., Pasquini L., Guenther E. W., Hartmann M., 2009b, A&A, 505, 1311
Drake S. A., Linsky J. L., 1983, ApJ, 274, L77
Drake S. A., Linsky J. L., 1986, AJ, 91, 602
Drake S. A., Linsky J. L., Elitzer M., 1987, AJ, 94, 1280
Drake S. A., Linsky J. L., Judge P. G., Elitzer M., 1991, AJ, 101, 230
Farrell W. M., Desch M. D., Zarka P., 1999, J. Geophys. Res., 104, 14025
Farrell W. M., Lazio T. J. W., Zarka P., Bastian T. J., Desch M. D., Ryabov B. P., 2004, Planet. Space Sci., 52, 1469
Frink S., Mitchell D. S., Quirrenbach A., Fischer D. A., Marcy G. W., Butler R. P., 2002, ApJ, 576, 478
Geier S., Edelmann H., Heber U., Morales-Rueda L., 2009, ApJ, 702, L96

Gillespie K. M. et al., 2008, Plasma Phys. Control. Fusion, 50, 124038
Griessmeier J.-M., Zarka P., Spreeuw H., 2007, A&A, 475, 359
Güdel M., 2002, ARA&A, 40, 217
Guillot T., Burrows A., Hubbard W. B., Lunine J. I., Saumon D., 1996, ApJ, 459, L35
Gurnett D. A., 1974, J. Geophys. Res., 79, 4227
Hatzes A. P., Cochran W. D., Endl M., McArthur B., Paulson D. B., Walker G. A. H., Campbell B., Yang S., 2003, ApJ, 599, 1383
Hatzes A. P., Guenther E. W., Endl M., Cochran W. D., Dollinger M. P., Bedalov A., 2005, A&A, 437, 743
Hatzes A. P. et al., 2006, A&A, 457, 335
Ignace R., 2001, PASP, 113, 1227
Jardine M., Cameron A. C., 2008, A&A, 490, 843
Jeans J. H., 1924, MNRAS, 85, 2
Johnson J. A., Marcy G. W., Fischer D. A., Henry G. W., Wright J. T., Isaacson H., McCarthy C., 2006, ApJ, 652, 1724
Johnson J. A. et al., 2007, ApJ, 665, 785
Johnson J. A., Marcy G. W., Fischer D. A., Wright J. T., Reffert S., Kregenow J. M., Williams P. K. G., Peek K. M. G., 2008, ApJ, 675, 784
Judge P. G., Stencel R. E., 1991, ApJ, 371, 357
Lamers H. J. G. L. M., Cassinelli J. P., 1999, Introduction to Stellar Winds. Cambridge Univ. Press, New York
Lammer H., Selsis F., Ribas I., Guinan E. F., Bauer S. J., Weiss W. W., 2003, ApJ, 598, L121
Lazio T. J. W., Farrell W. M., Dietrick J., Greenless E., Hogan E., Jones C., Hennig L. A., 2004, ApJ, 612, 511
Lazio J., Macdowall R. J., Burns J., DeMaio L., Jones D. L., Weiler K. W., 2007, to appear in Astrophysics Enabled by the Return to the Moon, preprint (astro-ph/0701770)
Li J., Ferrario L., Wickramasinghe D., 1998, ApJ, 403, L151
Linsky J. L., Haisch B. M., 1979, ApJ, 229, L27
Liu Y.-J. et al., 2008, ApJ, 672, 553
Livio M., Soker N., 1984, MNRAS, 208, 763
Livio M., Soker N., 2002, ApJ, 571, L161
Livio M., Pringle J. E., Saffer R. A., 1992, MNRAS, 257, 15
Luttermoser D. G., Brown A., 1992, ApJ, 384, 634
McConville S. L. et al., 2008, Plasma Phys. Control. Fusion, 50, 074010
Mutel R. L., Peterson W. M., Jaeger T. R., Scudder J. D., 2007, J. Geophys. Res., 112, 07211
Mutel R. L., Christopher I. W., Pickett J. S., 2008, Geophy. Res. Lett., 35, 07104
Niedzielski A. et al., 2007, ApJ, 669, 1354
Niedzielski A., Nowak G., Adamow M., Wolszczan A., 2009a, ApJ, 707, 768
Niedzielski A., Gozdziewski K., Wolszczan A., Konacki M., Nowak G., Zielinski P., 2009b, ApJ, 693, 276
Rasio F. A., Tout C. A., Lubow S. H., Livio M., 1996, ApJ, 470, 1187
Reffert S., Quirrenbach A., Mitchell D. S., Albrecht S., Hekker S., Fischer D. A., Marcy G. W., Butler R. P., 2006, ApJ, 652, 661
Reid M. J., Menten K. M., 1996, in Taylor A. R., Pardes J. M., eds, ASP Conf. Ser. Vol. 93, Radio Emission from the Stars and Sun. Astron. Soc. Pac., San Francisco, p. 87
Reimers D., 1975, Mem. Soc. R. Sci. Liège, 6e, Ser., 8, 369
Sato B. et al., 2003, ApJ, 597, L157
Sato B. et al., 2007, ApJ, 661, 527
Sato B. et al., 2008a, PASJ, 60, 539
Sato B. et al., 2008b, PASJ, 60, 1317
Schröder K.-P., Cuntz M., 2005, ApJ, 630, L73
Setiawan J. et al., 2003, A&A, 398, L19
Setiawan J. et al., 2005, A&A, 437, L31
Soker N., 2001, MNRAS, 324, 699
Soker N., Livio M., Harpaz A., 1984, MNRAS, 210, 189
Spergel D. N., Giuliani J. L. Jr, Knapp G. R., 1983, ApJ, 275, 330
Struck C., Cohanim B. E., Willson L. A., 2004, MNRAS, 347, 173
Suzuki T. K., 2007, ApJ, 659, 1592
Tsuji T., Unno W., Kaifu N., Izumiura H., Ukita N., Cho S., Koyama K., 1988, ApJ, 327, L23
Zarka P., 1998, J. Geophys. Res., 103, 20159
Zarka P., 2004, Planet. Space Sci., 52, 1455
Zarka P., 2007, Planet. Space Sci., 55, 598
Zarka P., Treumann R. A., Ryabov B. P., Ryabov V. B., 2001, Ap&SS, 277, 293
Zuckerman B., Becklin E. E., 1987, Nat, 330, 138

APPENDIX A: THERMAL CYCLOTRON EMISSION FROM THE BOW SHOCK

The steps for determining the radio flux density in the bow shock model is detailed. The differential luminosity $\mathrm{d}L$ of cyclotron emission from a small unit of volume $\mathrm{d}V$ is given by

$$\mathrm{d}L = \frac{\sigma_T}{6\pi c}\, v_\mathrm{e}^2\, B^2\, n_\mathrm{e}\, \mathrm{d}V, \tag{A1}$$

for thermal cyclotron emission by non-relativistic electrons. For an environment with a position dependent magnetic field, the frequency bandwidth of the emission is given by

$$\mathrm{d}\nu = \frac{e}{2\pi m_\mathrm{e} c}\, \mathrm{d}B. \tag{A2}$$

Thus, the specific luminosity becomes

$$L_\nu = \frac{\mathrm{d}L}{\mathrm{d}\nu} = \frac{1}{6\pi}\, \frac{\sigma_T\, v_\mathrm{e}^2}{c}\, \frac{B^3}{\nu_\mathrm{c}}\, n_\mathrm{e}\, \frac{\mathrm{d}V}{\mathrm{d}B}, \tag{A3}$$

where ν_c is the cyclotron frequency. For the bow shock model of Cassinelli et al. (2008), the EM *EM* is dominated in large part by the region along the bow shock. We can make the following approximation for the cyclotron emitting volume,

$$n_\mathrm{e}\, \mathrm{d}V = \frac{1}{n_\mathrm{e}}\, \mathrm{d}EM. \tag{A4}$$

This last expression takes advantage of the 'on the shock approximation' (OTSh) of Cassinelli et al. (2008), for which $n_\mathrm{e} \approx$ constant along the bow shock in the strong shock limit. This occurs under the assumption that the extent of the bow shock is relatively small compared to the orbital radius.

The specific luminosity of cyclotron emission now becomes

$$L_\nu = \frac{\sigma_T\, v_\mathrm{e}^2\, B^3}{6\pi n_\mathrm{e} c \nu_\mathrm{c}}\, \frac{\mathrm{d}EM/\mathrm{d}T}{\mathrm{d}B/\mathrm{d}T}, \tag{A5}$$

where we have taken $\mathrm{d}EM/\mathrm{d}B$ as a ratio of parametric form in the temperature T. Since T is a smoothly decreasing function along the bow shock surface, it acts effectively as a mapping coordinate in our prescription for the thermal cyclotron emission. The differential EM is simply a power law in temperature given by

$$\frac{\mathrm{d}EM}{\mathrm{d}T} = \frac{EM_0}{T_A}\, \left(\frac{T}{T_A}\right)^{-7/3}. \tag{A6}$$

In order to determine $\mathrm{d}B/\mathrm{d}T$, we require two pieces of information. The first is how the field varies in space around the companion object. We will assume that the field is a dipole. Since we are seeking mainly an order of magnitude estimate of the emission level at long wavelengths in the radio, we will ignore latitudinal variations of the field and simply adopt $B = B_0\,(R/r)^3$, where R is the companion radius. The second piece is the mapping of $r(T)$ along the bow shock as it cuts through the dipole field. From Cassinelli et al. (2008), the bow shock shape is close to a parabola (especially near the bow head, that is most relevant for our work), which is a convenient form to work with. Again, with the goal of obtaining an order of magnitude estimate, we approximate the bow shock geometry using

$$z = z_0 + a\, R\, \left(\frac{\varpi}{R}\right)^2, \tag{A7}$$

where $z_0 = 1.19\ R$ and $a = 0.35$, where (ϖ, z) are cylindrical coordinates for the axisymmetric bow shock with z the symmetry axis. The way to obtain $B(T)$ is a two step process. The first step is to derive $r(\varpi)$; the second is to use $\varpi(T)$ from Cassinelli et al.

With $r^2 = z^2 + \varpi^2$, the solution for $r(\varpi)$ is derived from a quartic relation in $\varpi(r)$ that can be inverted to obtain r itself; the result is

$$\frac{r(\varpi)}{R} \approx \sqrt{1.4 + 5.7\varpi^2 + 1.1\varpi^4}. \tag{A8}$$

The solution for $\varpi(T)$ is approximately given by

$$\frac{\varpi(T)}{R} \approx \left[\frac{3}{2}\left(\frac{T_A}{T} - 1\right)\right]^{3/8}. \tag{A9}$$

Finally, the end result for $\mathrm{d}B/\mathrm{d}T$ can be compactly expressed as

$$\frac{\mathrm{d}B}{\mathrm{d}T} \approx 9\left(\frac{R^2}{r^2}\right)\left(\frac{B}{T_A}\right)\xi\, x^{-2}, \tag{A10}$$

where

$$x = T/T_A \tag{A11}$$

and

$$\xi = \frac{1}{y^{1/4}} + \frac{1}{2}\, y^{1/2}, \tag{A12}$$

with

$$y = \frac{1}{x} - 1. \tag{A13}$$

For the electron velocity, we use the rms thermal value of

$$v_\mathrm{e} = \frac{2kT}{m_\mathrm{e}}. \tag{A14}$$

Combining the preceding relations, noting that the flux density is $S_\nu = L_\nu/4\pi D^2$ for distance D, and introducing a maximum frequency of emission ν_A corresponding to the apex of the bow shock that temperature T_A and minimum radius $r_A = r(T_A)$, the flux density becomes

$$S_\nu \sim 0.3\ \mu\mathrm{Jy}\left(\frac{B_0}{30\ \mathrm{G}}\right)\left(\frac{T_A}{30\,000\ \mathrm{K}}\right)\left(\frac{EM_0}{1.4\times10^{46}}\right) \times \left(\frac{n_\mathrm{e}}{5.7\times10^7}\right)^{-1}\left(\frac{D}{100\ \mathrm{pc}}\right)^{-2}\left(\frac{\nu}{\nu_A}\right)^{1/3} x^{2/3}\xi^{-1}. \tag{A15}$$

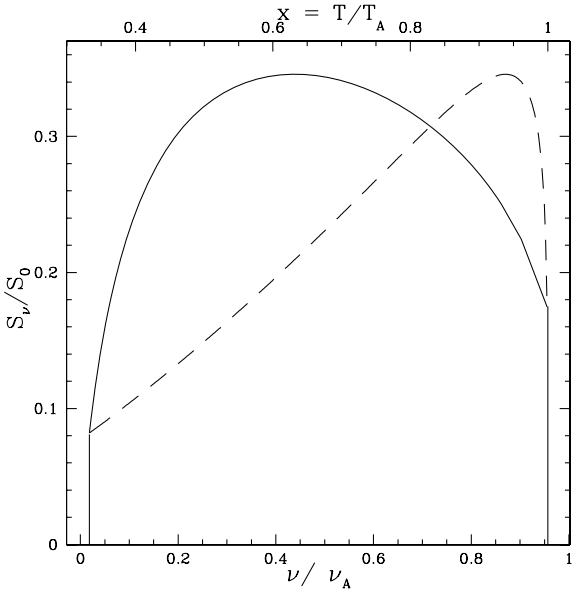

Figure A1. A plot of the radio spectrum with frequency (lower axis and solid curve) and temperature (upper axis and dashed curve). The temperature ranges from the apex value T_A down to a lower cut-off corresponding to the shock being too weak to ionize H, here taken as $0.4T_A$. Since the bow shock penetrates deepest into the magnetosphere, the highest temperature point is likely to sample the highest magnetic field value corresponding to emission at frequency ν_A. The spectrum is illustrative only, as it assumes $B \propto r^{-3}$ without taking any account of latitudinal dependence.

The total emission is sub-micro-Jansky and peaks close to the maximum frequency. An example spectrum is shown in Fig. A1. The flux density is normalized to 0.3 μJy with nominal values assumed for the physical parameters in equation (A15). The lower temperature bound is taken as $T_0 = 10\,000$ K. The solid curve is the for the frequency spectrum; the dashed curve plots the emission against the temperature distribution with scale given at the top. It is assumed that hydrogen is completely ionized over this temperature range.

This paper has been typeset from a TEX/LATEX file prepared by the author.